Geophysical Research Letters

RESEARCH LETTER
10.1029/2024GL108405

Brittle-Ductile Rheological Behavior in Subduction Zones: Effects of Strength Ratio Between Strong and Weak Phases in a Bi-Phase System

A. Maitre[1], F. Gueydan[1], C. Thieulot[2], and E. Oliot[1]

[1]Geosciences Montpellier, Université de Montpellier, CNRS, Montpellier, France, [2]Earth Sciences, Utrecht University, Utrecht, The Netherlands

Key Points:

- The modeled brittle-ductile rheological behavior occurs in a more limited temperature range than theoretically predicted
- The strength ratio between the brittle yield stress and the dislocation creep stress predicts conditions for the brittle-ductile behavior
- The temperature, pressure and pore-fluid pressure conditions for the brittle-ductile behavior are those of the deep transient slips

Supporting Information:

Supporting Information may be found in the online version of this article.

Correspondence to:

A. Maitre,
antoine.maitre@umontpellier.fr

Citation:

Maitre, A., Gueydan, F., Thieulot, C., & Oliot, E. (2024). Brittle-ductile rheological behavior in subduction zones: Effects of strength ratio between strong and weak phases in a bi-phase system. *Geophysical Research Letters*, *51*, e2024GL108405. https://doi.org/10.1029/2024GL108405

Received 18 JAN 2024
Accepted 11 APR 2024

Abstract The brittle-ductile rheological behavior in subduction zones is commonly proposed to explain deep transient slips. Generally observed at large scales in tectonic "mélanges", here we show that it is also observed at the grain scale in exhumed blueschist metagabbros. In these rocks, petrologic and microstructural observations show a bi-phase material constituted by strong microfractured magmatic pyroxene clasts located in a weak and ductile lawsonite-rich metamorphic matrix. To constrain the mechanical conditions allowing the brittle deformation of a clast in a ductile matrix, we used two-dimensional simple shear numerical experiments. Results show four behaviors: (a) entirely brittle; (b) brittle-ductile with clast fracturing in a ductile matrix; (c) ductile-dominant with limited plastic deformation at clast edges; and (d) entirely ductile. We propose that the conditions of the brittle-ductile behavior, commonly associated with deep transient slips, are controlled by the strength ratio between the strong brittle phase and the weak ductile phase.

Plain Language Summary In subduction zones, brittle-ductile behavior is commonly proposed to explain deep transient slips at the subduction interface. This particular behavior is generally characterized by the fracturing of strong pods located in a weak fluid-like material. In this study, we observe this mixed rheological behavior at the mineral-scale in oceanic rocks under deep transient slip conditions. We carry out petrological and microstructural observations that show micro-fracturing of strong magmatic clasts and ductile deformation of a weak metamorphic hydrated matrix. Numerical experiments, inspired by these observations, are used to constrain the physical conditions for this brittle-ductile behavior. Numerical results show four types of behavior: (a) both matrix and clast are brittle and fractured; (b) the clast is brittle and fractured and the matrix is ductilely deformed; (c) only the clast is brittle and fractures are localized at clast edges; and (d) both matrix and clast are ductile. This study demonstrates that the behavior of this bi-phase material is controlled by the strength ratio between the brittle strong clast and the ductile weak matrix. These physical conditions significantly differ from the theoretical rheological prediction and may be the key to a better understanding of the mechanics of deep transient slips.

1. Introduction

In subduction zones, slow slip events and non-volcanic tremors (called hereafter transient slips) question the rheological behavior of the plate interface (see review by Bürgmann (2018)). These signals are produced by occasional or periodic shear slips inside a ductile deformed volume in the presence of high pore fluid pressure (Shelly et al., 2006). In this study, we focus on the mechanics of deep transient slips, located at the transition between the locked domain (i.e., the seismogenic zone with a brittle behavior) and the creeping domain (i.e., aseismic zone with a ductile behavior) of the subduction interface. This transition occurs inside the subduction zone, approximately between 25 and 55 km depths, at temperatures comprised between 350 and 550°C (Behr & Bürgmann, 2021).

The classical geological signature of deep transient slips in blueschist to amphibolitic metamorphic conditions are filled fractures in centimetric to multi-metric lenses of mafic rock (i.e., oceanic material) inside metasediments and/or serpentinites (Behr & Bürgmann, 2021; Fagereng et al., 2014; Hayman & Lavier, 2014). The characteristic of this tectonic "mélange" is the existence of a brittle-ductile behavior in the bi-phase assemblage (e.g., Handy et al., 1999, and reference therein; Jammes et al., 2015; Lavier et al., 2021), characterized by a brittle deformation of stronger mafic lenses and a ductile deformation of the weaker matrix. Fractures in strong lenses are usually filled by hydrated mineral (e.g., amphiboles), quartz and/or carbonates suggesting fluid circulations under high pore fluid

pressure conditions (Angiboust et al., 2015; Kotowski & Behr, 2019). In bi-phase continental rocks, brittle-ductile behavior has been observed at the grain scale, with brittle strong feldspars located in a weak ductile quartz (±micas) matrix (Ioannidi et al., 2022; Jammes et al., 2015). It was also proposed to trigger transient ductile strain localization (i.e., transient slip) enhanced by fracturing and fluid flow (Bernaudin & Gueydan, 2018). In oceanic material, brittle-ductile behavior has been identified in eclogitic conditions, with fracturing of strong garnet in weaker omphacite-rich matrix (Yamato et al., 2019). In this study, we identify brittle-ductile behavior in a metagabbro deformed at blueschist facies conditions (i.e., at deep transient slips conditions, Bürgmann, 2018).

Previous numerical models have shown that such bi-phase systems with brittle-ductile behavior can effectively lead to transient slips (Beall et al., 2019; Behr et al., 2021; Hayman & Lavier, 2014). The presence of the weak and ductile matrix around the strong phase limits the rupture propagation and therefore explains the slow rupture (Hayman & Lavier, 2014). The fracturing of the strong phases, and hence potentially the occurrence of transient slips, is controlled by the proportion of the strong phases and the matrix viscosity (Behr et al., 2021; Fagereng & Beall, 2020; Ioannidi et al., 2021). In addition, the interaction between frictional deformation of strong clasts can localize strain and thus explain transient slips (Beall et al., 2019).

In this study, we wish to identify what constrains the depth distribution of such brittle-ductile rheological behavior at subduction plate interfaces, and to specify the physical parameters that control this particular behavior. To do so, we use 2D numerical model that represents a simple bi-phase system inspired by the deformation microstructures observed in metagabbros. This modeling results show that the strength ratio between the brittle yield stress of the clast and the ductile strength of the matrix controls the existence of the brittle-ductile rheological behavior at the subduction interface.

2. Materials and Methods

2.1. Geological Constraints From Deformed Blueschist Metagabbros (Queyras, Alps, France)

We used two samples (EQ2002, Figures 1a and 1b and EQ2005, Figures 1c and 1d) of blueschist metagabbros from the Schistes Lustrés complex in the Queyras massif (oceanic-derived metamorphic units) in the Western Alps (Agard, 2021). These metagabbros are part of main mafic lenses (metric to kilometric) included in metasediments. EQ2002 presents a moderate deformation, while EQ2005 shows more pronounced deformation with numerous shear bands, both developed under blueschist conditions. Peak P-T conditions in this area have been estimated at 350–400°C and 13–17 kb (Herviou et al., 2021), equivalent to the conditions where transient slips occur.

In EQ2002 (Figure 1a–1b), a weak foliation is present and is marked by aligned metamorphic blue amphiboles (i.e., glaucophane). Large magmatic pyroxene (i.e., diopside) is altered and stretched with numerous microfractures, oriented orthogonal to the stretching direction and filled by actinolite or glaucophane. Pressure shadows around diopside porphyroclasts are filled by glaucophane. Plagioclase (albite) is no longer stable at blueschist facies conditions, and replaced by fine-grained lawsonite. Newly crystallized metamorphic minerals (hydrated minerals: glaucophane and lawsonite) present in the fine-grained and ductilely deformed matrix testify for a large fluid supply during the burial (Condit et al., 2020; Hacker et al., 2003) and widespread microfractures suggest the overpressure of these fluids (Angiboust et al., 2012). Late fractures filled by albite crosscut the blueschist foliation and thus mark the exhumation through retrograde greenschist facies conditions with large fluid circulation and overpressure (Agard et al., 2000).

In EQ2005 (Figures 1c and 1d), ductile deformation and metamorphic transformation are more pronounced, as shown by the high density of localized shear bands and the abundance of glaucophane and lawsonite, neocrystallized at the expense of all magmatic pyroxene (diopside) and plagioclase. Pyroxene still occurs as metamorphic (stable) omphacite. Local shear bands are marked by glaucophane and calcite with a pronounced fracturing of pyroxene. Fractures of the whole rock occur and are filled by calcite. These fractures are open joints in pyroxenes associated with the shearing and glaucophane crystallization, therefore also occurring during blueschist deformation. These fractures testify for fluid circulation and fluid overpressure with fluid composed of H_2O (hydrated minerals) and CO2 (carbonate minerals).

From these observations, we can conclude that deformation of metagabbros at blueschist facies conditions is marked by the intense fracturing of magmatic pyroxenes and the ductile deformation of a fine-grained matrix, made of a hydrated assemblage of lawsonite and glaucophane. Fluid circulations and prograde metamorphic

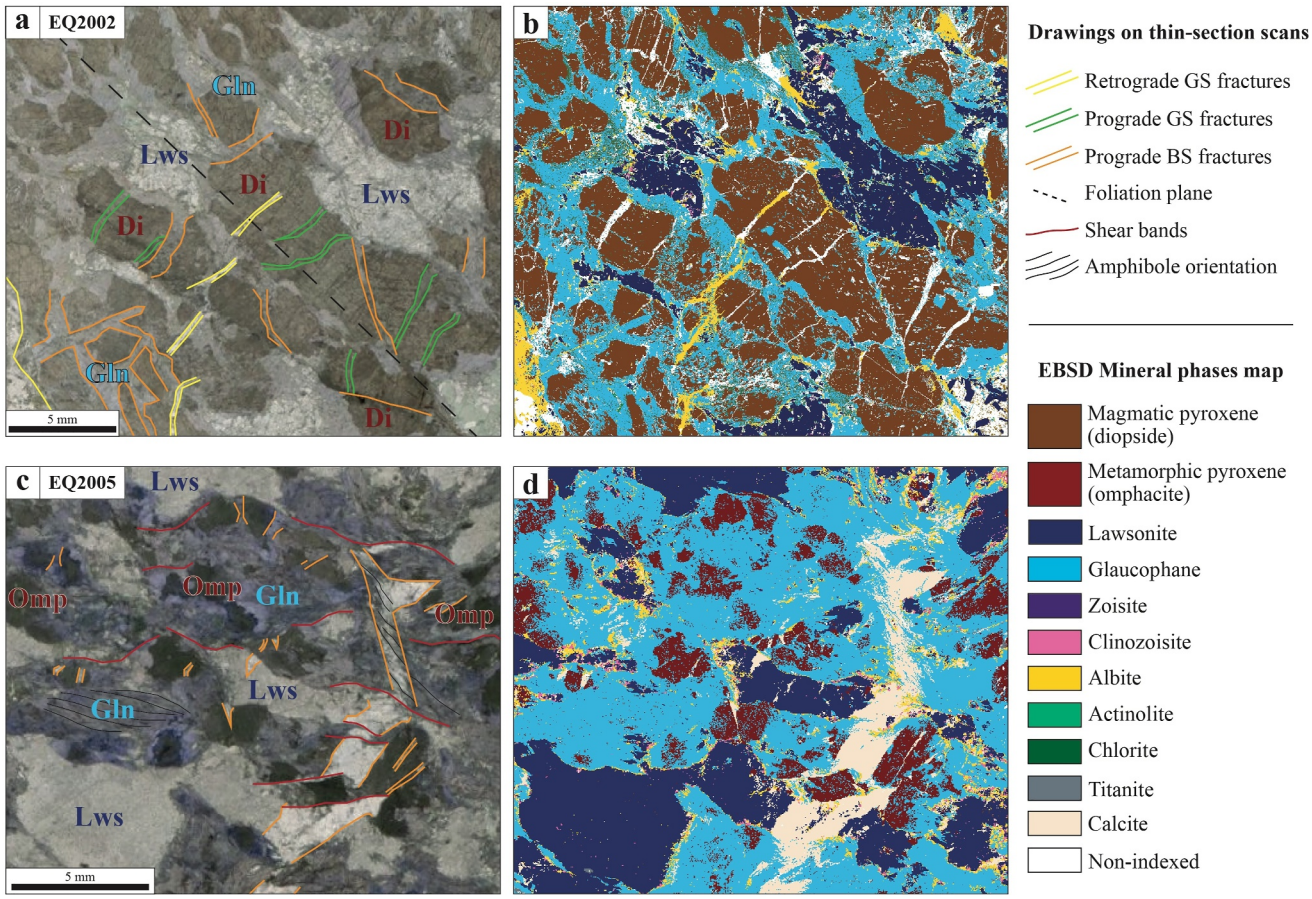

Figure 1. Typical microstructures in blueschist metagabbros from the Queyras Massif (French Alps, location in Figure S1 in Supporting Information S1). (a and c) Optical photomicrographs and (b and d) mineral phase maps from EQ2002 (onset of ductile deformation) and EQ2005 (more deformed with blueschist shear bands), respectively. The phase maps have been obtained by crystallographic analyses (Electron Backscattered Diffraction). The weak foliation in EQ2002 is highlighted by a black dotted line.

reactions in the presence of fluids are associated with this brittle-ductile deformation (pyroxene clasts + H_2O = amphiboles; and chlorite + actinote + albite + H_2O in matrix = glaucophane + lawsonite for the matrix). For larger finite strain, a more pronounced fracturing of magmatic pyroxenes and their replacement by metamorphic minerals (glaucophane, omphacite) occurs.

We simplify this natural example with a two-phase system composed of a simple pyroxene clast (modeled by a disc) located inside a weaker matrix. The matrix will be modeled as an assemblage of albite and amphibole, representative of the prograde greenschist facies deformation and metamorphism (prior to the main blueschist event).

2.2. Model Set-Up and Rheologies

The model set-up represents an idealized gabbro as a square (1 cm in size) sustaining simple shearing, at a constant temperature, confining lithostatic pressure and pore fluid pressure. The domain contains a circular inclusion (radius of 0.25 cm) and a surrounding matrix (Figure 2a). The inclusion is a pyroxene clast, and the matrix is an assemblage of plagioclase and amphiboles. We use the biotite dislocation creep law to model the weak amphibole flow law in the absence of dislocation creep data for wet amphibole and because biotite well reproduce the wet glaucophane strength that is significantly weaker than dry glaucophane with the brittle-ductile transition at relatively low pressure and temperature (see discussion in Kim et al. (2015) and Figure S2 in Supporting Information S1). The percentage of inclusion (i.e.,; pyroxene) was chosen at 20% of the box surface by comparison with the petrological observations of the studied metagabbros (Figure 1). Computations were done using

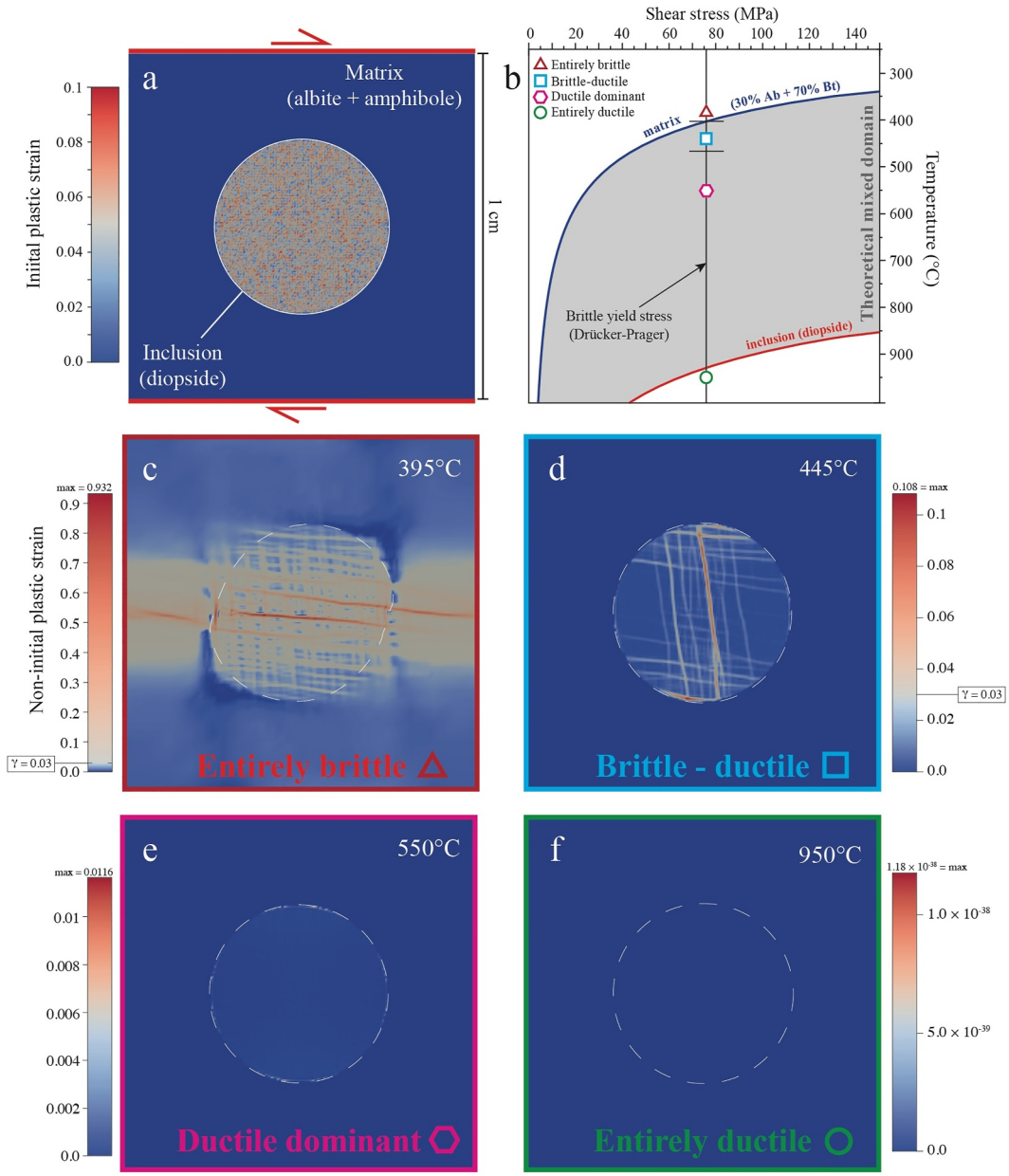

Figure 2. 2D numerical models. (a) Model set-up with a square (1 cm × 1 cm) sustaining simple shear at a constant velocity (background strain rate), temperature, pore fluid pressure and depth. Bi-phase system (inspired from microstructures in Figure 1): inclusion (diopside) as a perfect centered circle with randomly distributed initial plastic strain and matrix with a mixture of albite and amphibole. (b) Rheological profile (shear stress as a function of temperature) with dislocation creep flow stresses for the matrix (blue) and the inclusion (red) and the brittle (=plastic) yield stress (black, represented as a vertical line since the depth and pore fluid pressure is constant here). Markers for the four presented 2D models as circles: In (c), (d), (e) and (f), Non-initial plastic strain for four different temperatures, at 40 km depth, a strain rate of 10^{-12} s^{-1} and pore fluid pressure factor of 0.9 after a finite shear strain of 0.03. (c) At 395°C, entirely brittle model (brittle deformation in both the inclusion and the surrounding matrix). (d) At 445°C, brittle-ductile model (brittle deformation only in the inclusion and ductile deformation in the matrix). (e) At 550°C, ductile-dominant model (very limited brittle deformation at the edge of the inclusion accommodating its rotation in the ductile matrix). (f) At 950°C, entirely ductile model (ductile deformation in both the inclusion and the matrix). In (c), (d), (e) and (f), the white dotted circle is the inclusion contour.

the geodynamical finite element Advanced Solver for Planetary Evolution, Convection, and Tectonics ASPECT code version 2.5.0 (Bangerth et al., 2022, 2023; Gassmöller et al., 2018; Heister et al., 2017; Kronbichler et al., 2012). The rheological model combines dislocation creep and Drucker-Prager plasticity. The equations, as

well as the numerical and rheological parameters are provided in Text S1 and Figure S2 of Supporting Information S1.

The brittle behavior follows a Drucker-Prager criterion with a 30° angle of internal friction and a 20 MPa cohesion. Plastic strain weakening is used to trigger plastic strain localization (the angle of internal friction and the cohesion decrease to 0.1 times their initial values for plastic strain comprised between 0 and 0.5). The inclusion has a randomly distributed initial plastic strain to trigger plastic strain localization (Figure 2a). Note that these initial values do not modify the type of fracturing that we will discuss later.

The reference model is at a strain rate of 10^{-12} s^{-1} (typical of transient slip), a depth of 40 km and a pore fluid pressure coefficient of 0.9. We then vary the strain rate (from 10^{-14} s^{-1} to 10^{-11} s^{-1}), the temperature (320–1,000°C), the depth (25–55 km) and the pore fluid pressure (0.8–0.95). The final shear strain is limited to 0.03 to only depict deformation style at onset of deformation (Figure 2).

3. 2D Numerical Results

In this section, we first present the results for the reference model (40 km depth; pore fluid pressure equals to 0.9 time the lithostatic one, and strain rate fixed at 10^{-12} s^{-1}) at different temperatures, and then the parametric study (varying depths, pore fluid pressures, strain rates and temperatures).

3.1. The Four Rheological Behaviors

In theory, the deformation of the biphasic system should be described by three types of rheological behaviors (Figure 2b). (a) An entirely brittle rheological behavior (both matrix and inclusion are brittle) when the brittle yield stress (constant because the depth, fluid pressure, and strain rate are constant in the reference model) is lower than the dislocation creep flow stress (e.g., for temperature lower than 402.5°C, the temperature of the brittle-ductile transition of the matrix, Figure 2b). (b) An entirely ductile rheological behavior (both matrix and inclusion are ductile) when the dislocation creep flow stress of the inclusion is lower than the brittle yield stress (e.g., for temperature larger than 928.5°C, the temperature of the brittle-ductile transition of the pyroxene, Figure 2b). (c) In between, a brittle-ductile behavior (ductile matrix and brittle inclusion) should occur (e.g., for temperature between 402.5 and 928.5°C, gray domain in Figure 2b). Figure 2 presents four models, at 395°C (theoretically entirely brittle), 445°C (theoretically brittle-ductile), 550°C (theoretically brittle-ductile) and 950°C (theoretically entirely ductile) after a finite shear of 0.03.

At 395°C (Figure 2c) a brittle shear band initiates through the entire inclusion and the matrix from the first stages of deformation, as theoretically expected. This model corresponds to what we will call brittle models and corresponds to fracture development in both the inclusion and the matrix. The plastic strain reaches values (close to 1) that are larger than the imposed shear strain (0.03), typical of strain localization in brittle shear bands (Figure 2c). Most brittle models stop before the final execution time because of numerical instabilities related to the formation of brittle shear bands throughout the model and the very important local increase of strain rate. At 445°C (Figure 2d), the inclusion is plastically deformed with numerous brittle shear bands while the matrix is entirely ductile. This model corresponds to the brittle-ductile model, with an internal brittle deformation of the inclusion and a ductile matrix. Plastic strain localization occurs in the inclusion, with large values of plastic strain (e.g., 0.25). At 550°C (Figure 2e), the brittle deformation in the inclusion is very limited and only occurs at the edges of the inclusion. The maximum value of plastic strain is below the imposed shear strain, supporting the absence of plastic strain localization in the inclusion. In addition, the plastic strain is very low in the inner part of the inclusion, suggesting a rigid rotation of the inclusion in the ductile matrix (Figure S5 in Supporting Information S1). The plastic deformation at the grain edges accommodates this rotation. At this temperature, a brittle-ductile behavior was predicted (Figure 2a), but the absence of internal plastic deformation of the inclusion supports a ductile-dominant behavior. Finally, at 950°C (Figure 2f), no plastic deformation is observed both in the inclusion and in the matrix, as theoretically expected. This model corresponds to an entirely ductile model.

These 2D numerical results therefore illustrate four different types of rheological behavior of the bi-phase system, for increasing temperature as follows: entirely brittle, brittle-ductile, ductile-dominant, and entirely ductile. The brittle-ductile and ductile-dominant behaviors occur in the temperature conditions of the theoretical brittle-ductile behavior (Figure 2b).

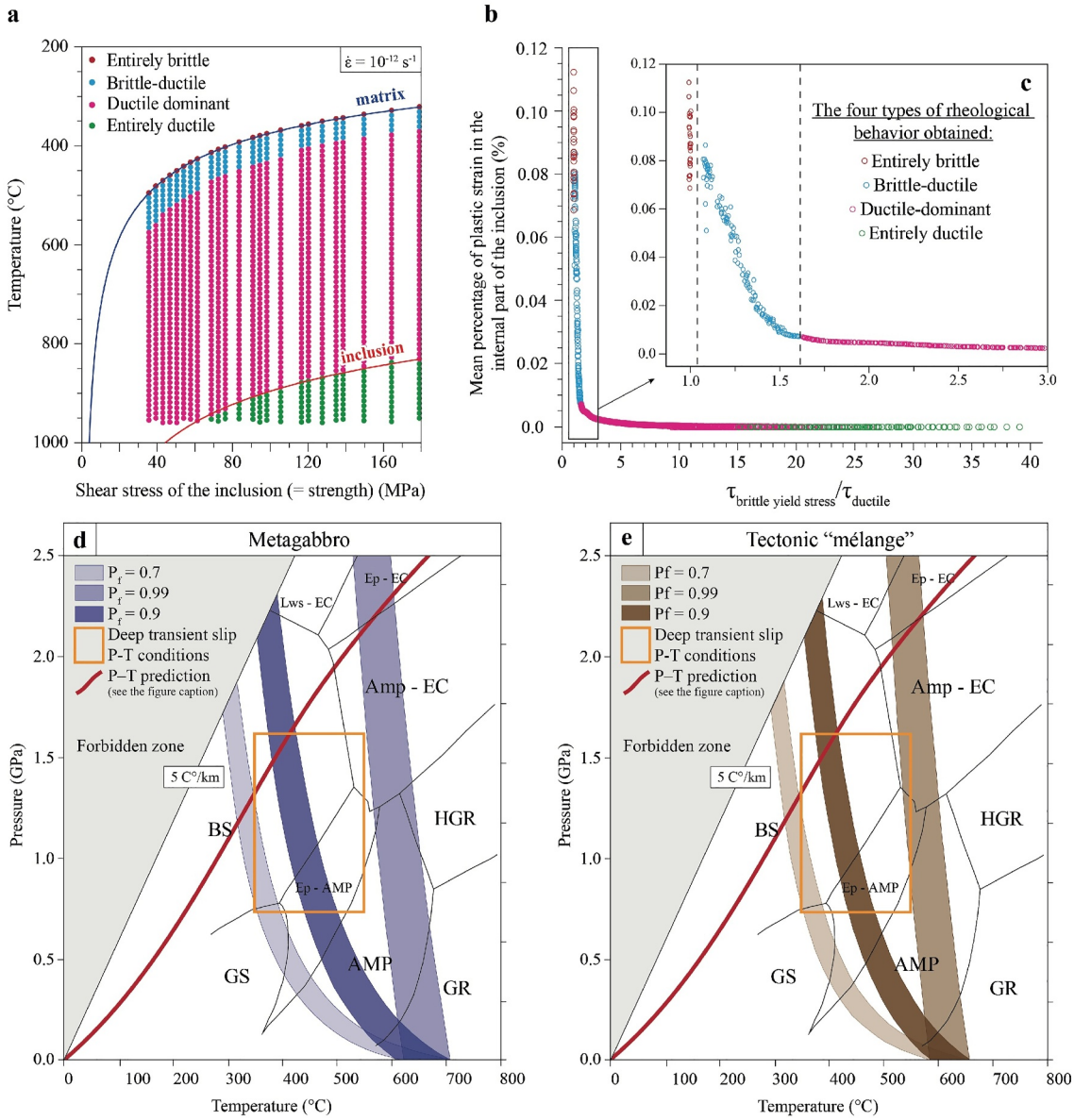

Figure 3. Parametric study for the characterization of the four previously inferred rheological behaviors. (a) Calculated strength profiles with matrix and inclusion ductile flow stresses. The vertical lines corresponds to different depths (25–55 km) and pore fluid pressure factors (0.8–0.95). Strain rate was fixed at 10^{-12} s^{-1}. 2645 model results presented as dots in red, blue, pink, and green for observed entirely brittle, brittle-ductile, ductile dominant, and entirely ductile behaviors, respectively. (b) Mean plastic strain in the inclusion as a function of the ratio between the yield brittle strength and the matrix ductile strength (obtained with the dislocation creep law of the matrix, Text S2 and Figure S2 in Supporting Information S1). (c) Close-up view showing the critical values of the strength ratio for predicting the limit between the entirely brittle behavior and the brittle-ductile behavior (ratio >1), and between brittle-ductile and ductile-dominant behaviors (ratio ≈ 1.6) (d) and (e) P-T diagrams displaying conditions for the occurrence of a brittle-ductile rheological behavior in a biphasic system, as a function of pore fluid pressure conditions (0.7, 0.9 and 0.99) calculated for a metagabbro (d) where the weak phase is an assemblage of albite and amphibole and the strong phase is the pyroxene, and for a tectonic "mélange" (e) where the weak phase is the metasediments and the strong phase is eclogitic mafic lenses. The metamorphic facies are: GS = Greenschist; BS = Blueschist; AMP = Amphibolite; GR = Granulite; HGR = High granulite; Amp-EC = Amphibolite-Eclogite; Ep-AMP = Epidote-Amphibolite; Lws-EC = Lawsonite-Eclogite; Ep-EC = Epidote-Eclogite. Orange rectangle corresponds to the deep transient slip conditions (see Bürgmann, 2018). Red curve corresponds to a typical subduction geotherm approximately equal to 8°C/km.

3.2. Strength Profiles: Rheological Behaviors as a Function of the Temperature

Figure 3a shows strength profiles with 2645 model results (varying temperatures, depths, and pore fluid pressures and at a given strain rate of 10^{-12} s^{-1}) in which the four inferred rheological models have been identified. The vertical lines correspond to different brittle yield stress at different depths and pore fluid pressures.

Entirely brittle models only occur when the brittle shear stress is lower than the ductile flow stress of the weak phase (e.g., above the ductile flow curve of the matrix), as theoretically predicted (Figure 2b). Entirely ductile models only occur when the ductile flow stress of the strong phase is lower than the brittle yield stress (e.g., below the ductile flow curve of the inclusion), as theoretically predicted (Figure 2b). The mixed brittle-ductile behaviors occur in a limited temperature range, located just below the brittle-ductile transition of the weak matrix.

This suggests that the strength of the inclusion and of the matrix need to be comparable to allow internal deformation and fracturing of the inclusion. Consistently, ductile-dominant behavior is observed for temperature conditions higher than those characteristics of the brittle-ductile transition of the matrix, allowing rigid rotation of the strong inclusion inside a weak matrix.

3.3. Strength Ratio: Prediction of the Rheological Behaviors

Figure 3b shows the mean plastic strain in the inclusion as a function of the ratio of the brittle yield stress over the ductile flow stress of the matrix. When the inclusion is brittle, the inclusion strength is controlled by the brittle yield stress that is a function of lithostatic pressure, friction coefficient and the cohesion (Glerum et al., 2018). The ratio of the brittle yield strength over the ductile matrix strength therefore represents the strength ratio between the inclusion and the matrix when the inclusion is brittle. This plastic strain/strength ratio curve also allows plotting all the 2645 model results in a single curve for varying temperatures, depths, pore fluid pressures, at a constant strain rate (10^{-12} s^{-1}).

The values of the mean plastic strain in the inclusion vary for the four inferred rheological behaviors. The entirely brittle behavior is marked by large values of plastic strain (e.g., plastic strain localization in the inclusion, Figure 2c) while the entirely ductile behavior is marked by zero plastic strain in the inclusion. The ductile dominant behavior occurs when plastic strain in the inclusion is limited (compare to the overall shear strain), and the brittle-ductile behavior arises when the mean plastic strain is large compared to the overall shear strain (marking plastic strain localization). Based on the visualization of all the calculated models, we propose that the limit between the brittle-ductile and the ductile dominant models occurs when the mean plastic strain in the internal part of the inclusion (80% of the inclusion) is lower than 25% the imposed shear strain (0.0075 in our case with 0.03 of imposed shear strain).

Brittle models have a strength ratio (brittle yield stress over the ductile matrix strength) less than or equal to one and a large mean plastic strain in the inclusion (Figure 3b). Ductile models have a large ratio and a zero-plastic strain in the inclusion. Ductile-dominant models occur for ratios larger than one and with very low mean plastic strain in the inclusion. Brittle-ductile models occur for ratios larger than one but close to one and with a variable mean plastic strain in the inclusion (from large values typical of brittle models to low values typical ductile dominant models). This parametric study allows constraining the values of the strength ratio that defines the transition from the brittle-ductile behavior to the ductile dominant behavior. This transition occurs when the plastic strain/strength ratio curve slope changes, from a steep slope in brittle-ductile models with decreasing plastic strain and increasing strength ratio, to an asymptotic sub-horizontal slope in ductile-dominant models with very limited to zero strain independently on the strength ratio (Figure 3b). Based on the all calculated models, the critical strength ratio for the transition between brittle-ductile behavior to ductile-dominant behavior is 1.6 (Figure 3c). This transition is independent of the strain rate (Figure S6 in Supporting Information S1) and the critical value of the strength ratio slightly depends on the proportion of strong phases (Figure S7 in Supporting Information S1).

The strength ratio between the brittle yield stress and the ductile matrix strength is therefore a robust proxy to predict the transition between the four inferred rheological behaviors: (a) brittle for ratio less than and equal to 1; (b) brittle-ductile for ratio greater than 1 and lesser than 1.6; (c) ductile-dominant for ratio higher than 1.6 and an internal plastic strain of the inclusion greater than 0.0; and (d) entirely ductile for larger ratio and internal plastic strain of the inclusion equal to 0.0.

Consequently, based on the values of the strength ratio, it is possible to predict the P-T conditions for the four rheological behaviors predicted in a metagabbro (Figure 3d). Brittle-ductile behavior is predicted to occur for limited P-T conditions in the blueschists to amphibolite conditions. In subduction settings (HP-LT metamorphic gradients), the brittle-ductile behavior implies P-T conditions consistent with estimated P-T conditions of transient slips. This rheological stratification (brittle, brittle-ductile, ductile-dominant, and

ductile) in bi-phase systems can therefore be a key to understand the parameters that control the seismogenic stratification in subduction zone. The difference between internal grain deformation (brittle-ductile behavior) and rigid grain rotation (ductile-dominant) is a key to explain why brittle-ductile behavior is limited in temperature and depths.

4. Discussion and Conclusion

Most previous studies have discussed the depth and temperature range of the brittle-ductile behavior as constrained by the onset of ductile flow in both the weak phase and the strong phase (see Handy et al., 1999 for a discussion). The novelty of our analysis is to demonstrate through numerical modeling that in bi-phase system, the "real" brittle-ductile behavior is even more restricted and controlled by the ratio between the brittle yield stress and the weak phase strength. This implies that the strength of the weak phase is a key controlling parameter of the rheology of a bi-phase system (Handy et al., 1999). Numerical models have also more precisely shown that the inclusion proportion may also control the bi-phase rheology but for a proportion larger than 50% (Beall et al., 2019). We can therefore propose that our analysis applies only for a bi-phase system with strong phase proportions lower than 50%, as also supported by our parametric study (Figure S7 in Supporting Information S1). Contact between inclusions will indeed slightly modify our results for larger proportion of strong clasts (Behr et al., 2021; Fagereng & Beall, 2020; Lavier et al., 2021).

Contact between strong clasts in a bi-phase system also leads to local stress concentration that can ultimately lead to formation of stress chains if contacts are important and connected. This stress chains can trigger local increase of slip (Reber et al., 2014) and hence transient slips (Fagereng & Beall, 2020). More generally, in these bi-phase systems, the triggering of velocity weakening frictional behavior in the strong phase is assumed to lead to slip instability and hence transient creep (Behr et al., 2021; Hayman & Lavier, 2014; Reber et al., 2015). In this study, we propose that the inferred brittle-ductile rheological behavior with fracturing of the clast inside a ductile matrix can be associated with transient slips. In addition, the dynamic fracturing of the strong phase can generate high deformation rates that can trigger brittle deformation in the weak matrix providing another mechanism for transient slips.

The limited P-T conditions for the existence of such brittle-ductile rheology is furthermore consistent with the limited depth and temperature extend of the transient slips in subduction zones (Figure 3d). The P-T conditions for the brittle-ductile rheological behavior strongly depends on the pore fluid pressure (Figure 3d). For large P_f, brittle-ductile behavior are predicted inside the transient slip domain ($P_f > 0{,}9 \times P_{lith}$, Figure 3d); while low P_f implies brittle-ductile behavior at low pressure and low temperature (outside the deep transient slip domain, $P_f = 0{,}7 \times P_{lith}$, Figure 3d). Consistently, transient slips are supposed to occur for very high pore fluid pressue ($P_f = 0{,}99 \times P_{lith}$, Behr & Bürgmann, 2021). The exact P-T conditions for brittle-ductile behavior at very high pore pressure also depends on the matrix rheology (mineral phases, Figure S8 in Supporting Information S1). The state of fluids, the variation in pore fluid pressure and the associated metamorphic reaction along the subduction plate interface will therefore be a key controlling factor in determining the depth extent of the brittle-ductile behavior. Our numerical results are a first step to better constrain such complex behavior.

Our results can also be extrapolated to larger scale with a subduction plate interface made of meter to kilometer scale lenses of strong mafic rocks embedded in a weak metasedimentary rock (tectonic "mélange", see for example Kotowski & Behr, 2019). Using flow laws for mafic and metasedimentary materials, we can calculate the P-T conditions for the existence of brittle-ductile behavior in such tectonic "mélange", based on the critical strength ratios defined in this study (brittle stress over the ductile stress of the matrix, here metasediments). The P-T conditions are very similar to the one calculated for metagabbro, exemplifying the role of the matrix rheology (here metasediments) and the role of pore fluid pressure in defining the brittle-ductile behavior (Figure 3e). More generally, our study therefore supports that the deformation of a bi-phase system (at grain scale or at meter to kilometer scale) can explain the rheological distribution at the subduction plate interface: a brittle behavior (seismogenic, at low P-T), a brittle-ductile behavior (predicted in limited P-T conditions) marked by fracturing of the strong phase and ductile creeping of the weak phase, likely associated with transient slips, and a ductile behavior marked by either dominant creeping with limited plastic deformation or fully ductile behavior at larger temperatures and depths.

Data Availability Statement

We use the open source code ASPECT 2.5.0 (Bangerth et al., 2022, 2023; Heister et al., 2017; Kronbichler et al., 2012) published under the GPL2 license. The input file and the bash script file that generate and run all the models shown in this manuscript can be accessed in Mendeley data set (Maitre et al., 2024).

Acknowledgments
We thank to C. Nevado and D. Delmas for thin sections preparation and to F. Barou for EBSD data acquisition. We thank the Computational Infrastructure for Geodynamics (http://geodynamics.org) which is funded by the National Science Foundation under awards EAR-0949446, EAR-1550901, and EAR-2149126. We thank Jacqueline Reber and Luc Lavier for their constructive reviews and the editor Quentin Williams for his editorial handling.

References

Agard, P. (2021). Subduction of oceanic lithosphere in the Alps: Selective and archetypal from (slow spreading) oceans. *Earth-Science Reviews*, *214*, 103517. https://doi.org/10.1016/j.earscirev.2021.103517

Agard, P., Goffé, B., Touret, J. L. R., & Vidal, O. (2000). Retrograde mineral and fluid evolution in high-pressure metapelites (Schistes lustrés unit, Western Alps). *Contributions to Mineralogy and Petrology*, *140*(3), 296–315. https://doi.org/10.1007/s004100000190

Angiboust, S., Agard, P., Yamato, P., & Raimbourg, H. (2012). Eclogite breccias in a subducted ophiolite: A record of intermediatedepth earthquakes? *Geology*, *40*(8), 707–710. https://doi.org/10.1130/G32925.1

Angiboust, S., Kirsch, J., Oncken, O., Glodny, J., Monié, P., & Rybacki, E. (2015). Probing the transition between seismically coupled and decoupled segments along an ancient subduction interface. *Geochemistry, Geophysics, Geosystems*, *16*(6), 1905–1922. https://doi.org/10.1002/2015GC005776

Bangerth, W., Dannberg, J., Fraters, M., Gassmoeller, R., Glerum, A., Heister, T., et al. (2022). ASPECT: Advanced solver for problems in Earth's convection, User Manual. https://doi.org/10.6084/M9.FIGSHARE.4865333

Bangerth, W., Dannberg, J., Fraters, M., Gassmoeller, R., Glerum, A., Heister, T., et al. (2023). Geodynamics/aspect: ASPECT 2.5.0 (version v2.5.0). https://doi.org/10.5281/ZENODO.8200213

Beall, A., Fagereng, Å., & Ellis, S. (2019). Strength of strained two-phase mixtures: Application to Rapid creep and stress amplification in subduction zone mélange. *Geophysical Research Letters*, *46*(1), 169–178. https://doi.org/10.1029/2018GL081252

Behr, W. M., & Bürgmann, R. (2021). What's down there? The structures, materials and environment of deep-seated slow slip and tremor. *Philosophical Transactions of the Royal Society A*, *379*(2193), 20200218. https://doi.org/10.1098/rsta.2020.0218

Behr, W. M., Gerya, T. V., Cannizzaro, C., & Blass, R. (2021). Transient slow slip characteristics of frictional-viscous subduction megathrust shear zones. *AGU Advances*, *2*(3), e2021AV000416. https://doi.org/10.1029/2021av000416

Bernaudin, M., & Gueydan, F. (2018). Episodic tremor and slip explained by fluid-enhanced microfracturing and sealing. *Geophysical Research Letters*, *45*(8), 3471–3480. https://doi.org/10.1029/2018GL077586

Bürgmann, R. (2018). The geophysics, geology and mechanics of slow fault slip. *Earth and Planetary Science Letters*, *495*, 112–134. https://doi.org/10.1016/j.epsl.2018.04.062

Condit, C. B., Guevara, V. E., Delph, J. R., & French, M. E. (2020). Slab dehydration in warm subduction zones at depths of episodic slip and tremor. *Earth and Planetary Science Letters*, *552*, 116601. https://doi.org/10.1016/j.epsl.2020.116601

Fagereng, Å., Hillary, G. W. B., & Diener, J. F. A. (2014). Brittle-viscous deformation, slow slip, and tremor. *Geophysical Research Letters*, *41*(12), 4159–4167. https://doi.org/10.1002/2014GL060433

Fagereng, Å. A., & Beall, A. (2020). Is complex fault zone behaviour a reflection of rheological heterogeneity? *Philosophical Transactions of the Royal Society A: Mathematical, Physical & Engineering Sciences*, *379*(2193), 20190421. https://doi.org/10.1098/rsta.2019.0421

Gassmöller, R., Lokavarapu, H., Heien, E., Puckett, E. G., & Bangerth, W. (2018). Flexible and scalable particle-in-cell methods with adaptive mesh refinement for geodynamic computations. *Geochemistry, Geophysics, Geosystems*, *19*(9), 3596–3604. https://doi.org/10.1029/2018GC007508

Glerum, A., Thieulot, C., Fraters, M., Blom, C., & Spakman, W. (2018). Nonlinear viscoplasticity in ASPECT: Benchmarking and applications to subduction. *Solid Earth*, *9*(2), 267–294. https://doi.org/10.5194/se-9-267-2018

Hacker, B. R., Abers, G. A., & Peacock, S. M. (2003). Subduction factory 1. Theoretical mineralogy, densities, seismic wave speeds, and H_2O contents. *Journal of Geophysical Research*, *108*(B1), 2029. https://doi.org/10.1029/2001jb001127

Handy, M. R., Wissing, S. B., & Streit, L. E. (1999). Frictional-viscous flow in mylonite with varied bimineralic composition and its effect on lithospheric strength. *Tectonophysics*, *303*(1–4), 175–191. https://doi.org/10.1016/S0040-1951(98)00251-0

Hayman, N. W., & Lavier, L. L. (2014). The geologic record of deep episodic tremor and slip. *Geology*, *42*(3), 195–198. https://doi.org/10.1130/G34990.1

Heister, T., Dannberg, J., Gassmöller, R., & Bangerth, W. (2017). High accuracy mantle convection simulation through modern numerical methods—II: Realistic models and problems. *Geophysical Journal International*, *210*(2), 833–851. https://doi.org/10.1093/gji/ggx195

Herviou, C., Verlaguet, A., Agard, P., Locatelli, M., Raimbourg, H., Lefeuvre, B., & Dubacq, B. (2021). Along-dip variations of subduction fluids: The 30–80 km depth traverse of the Schistes Lustrés complex (Queyras-Monviso, W. Alps). *Lithos*, *394–395*, 394–395. https://doi.org/10.1016/j.lithos.2021.106168

Ioannidi, P. I., Bogatz, K., & Reber, J. E. (2022). The impact of matrix rheology on stress concentration in embedded brittle clasts. *Geochemistry, Geophysics, Geosystems*, *23*(3), e2021GC010127. https://doi.org/10.1029/2021GC010127

Ioannidi, P. I., Le Pourhiet, L., Agard, P., Angiboust, S., & Oncken, O. (2021). Effective rheology of a two-phase subduction shear zone: Insights from numerical simple shear experiments and implications for subduction zone interfaces. *Earth and Planetary Science Letters*, *566*, 116913. https://doi.org/10.1016/j.epsl.2021.116913

Jammes, S., Lavier, L. L., & Reber, J. E. (2015). Localization and delocalization of deformation in a bimineralic material. *Journal of Geophysical Research: Solid Earth*, *120*(5), 3649–3663. https://doi.org/10.1002/2015JB011890

Kim, D., Katayama, I., Wallis, S., Michibayashi, K., Miyake, A., Seto, Y., & Azuma, S. (2015). Deformation microstructures of glaucophane and lawsonite in experimentally deformed blueschists: Implications for intermediate-depth intraplate earthquakes. *Journal of Geophysical Research: Solid Earth*, *120*(2), 1229–1242. https://doi.org/10.1002/2014JB011528

Kotowski, A. J., & Behr, W. M. (2019). Length scales and types of heterogeneities along the deep subduction interface: Insights from exhumed rocks on Syros Island, Greece. *Geosphere*, *15*(4), 1038–1065. https://doi.org/10.1130/GES02037.1

Kronbichler, M., Heister, T., & Bangerth, W. (2012). High accuracy mantle convection simulation through modern numerical methods. *Geophysical Journal International*, *191*(1), 12–29. https://doi.org/10.1111/j.1365-246X.2012.05609.x

Lavier, L., Tong, X., & Biemiller, J. (2021). The mechanics of creep, slow slip events, and earthquakes in mixed brittle-ductile fault zones. *Journal of Geophysical Research: Solid Earth*, *126*(2), e2020JB020325. https://doi.org/10.1029/2020JB020325

Maitre, A., Gueydan, F., Thieulot, C., & Oliot, E. (2024). *Brittle-ductile rheological behavior in subduction zones: Effects of strength ratio between strong and weak phases in a bi-phase system*. Mendeley Data, V1. https://doi.org/10.17632/hfdxy6zwpx.1

Reber, J. E., Hayman, N. W., & Lavier, L. L. (2014). Stick-slip and creep behavior in lubricated granular material: Insights into the brittle-ductile transition. *Geophysical Research Letters*, *41*(10), 3471–3477. https://doi.org/10.1002/2014GL059832

Reber, J. E., Lavier, L. L., & Hayman, N. W. (2015). Experimental demonstration of a semi-brittle origin for crustal strain transients. *Nature Geoscience*, *8*(9), 712–715. https://doi.org/10.1038/ngeo2496

Shelly, D. R., Beroza, G. C., Ide, S., & Nakamula, S. (2006). Low-frequency earthquakes in Shikoku, Japan, and their relationship to episodic tremor and slip. *Nature*, *442*(7099), 188–191. https://doi.org/10.1038/nature04931

Yamato, P., Duretz, T., & Angiboust, S. (2019). Brittle/ductile deformation of eclogites: Insights from numerical models. *Geochemistry, Geophysics, Geosystems*, *20*(7), 3116–3133. https://doi.org/10.1029/2019GC008249

References From the Supporting Information

Balestro, G., Festa, A., & Dilek, Y. (2019). Structural architecture of the Western Alpine Ophiolites, and the Jurassic seafloor spreading tectonics of the alpine Tethys. *Journal of the Geological Society*, *176*(5), 913–930. https://doi.org/10.1144/jgs2018-099

Dimanov, A., & Dresen, G. (2005). Rheology of synthetic anorthite-diopside aggregates: Implications for ductile shear zones. *Journal of Geophysical Research*, *110*(B7). https://doi.org/10.1029/2004JB003431

Janjou, D. (2004). *Descriptif des Cartes géologiques à 1/50 000 format "vecteurs"*. BRGM/RP-53473-FR, 21.

Ji, S., & Martignole, J. (1994). Ductility of garnet as an indicator of extremely high temperature deformation. *Journal of Structural Geology*, *16*(7), 985–996. https://doi.org/10.1016/0191-8141(94)90080-9

Kronenberg, A. K., Kirby, S. H., & Pinkston, J. (1990). Basal slip and mechanical anisotropy of biotite. *Journal of Geophysical Research*, *95*(B12), 19257–19278. https://doi.org/10.1029/jb095ib12p19257

Lardeaux, J.-M. (2014). Deciphering orogeny: A metamorphic perspective examples from European alpine and Variscan belts: Part II: Variscan metamorphism in the French massif Central—A review. *Bulletin de la Societe Geologique de France*, *185*(5), 281–310. https://doi.org/10.2113/gssgfbull.185.5.281

Ranalli, C., & Murphy, D. C. (1987). Rheological stratification of the lithosphere. *Tectonophysics*, *133*(4), 281–295. https://doi.org/10.1016/0040-1951(87)90348-9

Rybacki, E., & Dresen, G. (2004). Deformation mechanism maps for feldspar rocks. *Tectonophysics*, *382*(3–4), 173–187. https://doi.org/10.1016/j.tecto.2004.01.006

Zhang, J., & Green, H. W. (2007). Experimental investigation of eclogite rheology and its fabrics at high temperature and pressure. *Journal of Metamorphic Geology*, *25*(2), 97–115. https://doi.org/10.1111/j.1525-1314.2006.00684.x